Transmission/Reflection Measurement and Near-Field Mapping Techniques for Passive Intermodulation Characterisation of Printed Lines

Aleksey P. Shitvov[(1)], Dmitry E. Zelenchuk[(1)], Torbjörn Olsson[(2)], Alexander G. Schuchinsky[(1)], Vincent F. Fusco[(1)]

[(1)]*The Institute of Electronics, Communications and Information Technology (ECIT), Queen's University of Belfast*
Northern Ireland Science Park, Queen's Road, Queen's Island, Belfast, BT3 9DT, United Kingdom
Email: a.shitvov@queens-belfast.ac.uk

[(2)]*Powerwave Technologies Sweden AB,*
Box 1155, 164 26 Kista, Sweden
Email: Torbjorn.Olsson@pwav.com

INTRODUCTION

Printed circuit boards (PCB) represent one of the major technological bases for manufacturing packaged components, devices and systems. In many high frequency applications, low level of passive intermodulation (PIM) produced by PCB materials is an essential requirement. However, the nature of PIM generation in PCB laminates is not fully understood, and the experimental evaluation of PIM products in printed circuits still needs further elaboration.

Conventional methods of PIM characterisation of microwave laminates are based on two-port measurements of the transmitted (forward propagating signal at the device output) and reflected (reverse propagating signal at the device input) PIM products generated in the microstrip line specimens fed by the two-tone high power signals, cf. [1]. In practice, only reverse PIM products are often measured because they can interfere with the useful signals. Indeed, the tone frequencies, being in the transmitter band, generate the reflected PIM products falling into the receiver band that desensitise the receiver and degrade the performance of the whole system. Different measurement schemes are employed to retrieve the parameters of the nonlinear response. These include spectral analysis of the intermodulation products, [2], sweeps of intermodulation frequency, [3], as well as sweeps of the fundamental carrier power or power ratio of the two carriers, [4] and [5]. In most instances, polynomial model of the nonlinear response is used, and PIM generation is described as a localised process, so that the observed behaviour, e.g. variations of PIM level in the frequency sweeps, is attributed to interference of the products from individual localised PIM sources, cf. [1] and [6].

However, in contrast to the localised PIM sources associated with imperfect point contacts, loose or contaminated connectors or soldered joints, the inherently distributed PIM phenomena in printed lines, [7], exhibit fundamentally different properties. Therefore, adequate characterisation of PIM production in printed circuits requires a special care. Although the conventional two-port transmission/reflection PIM measurements on printed lines still remain the reference technique for PIM characterisation of microwave laminates, its "black-box" representation of the device under test may be insufficient when applied to the distributed PIM phenomena. In such circumstances, near-field mapping of the PIM product distributions on printed traces permits reliable identification of the PIM generation mechanisms and location of isolated PIM sources, [8].

In this paper, the mechanisms of PIM generation are investigated using the two-port transmission/reflection PIM measurements and near-field mapping of distributed PIM products. In section 1, two different, though complementary, approaches to PIM characterisation of microwave laminates, referred to as Approach 1 and Approach 2, are described and the test results are compared for a reference laminate material. The details of the near-field mapping technique, implemented in the Approach 1, are presented in section 2. In section 3, the issues of comparability of the results obtained from the two-port and near-field measurements are discussed, and further compared with the distributed model of PIM generation, based upon the nonlinear transmission line (NTL) phenomenology, [7]. The main findings are summarised in Conclusion.

1. TWO-PORT TRANSMISSION/REFLECTION INTERMODULATION MEASUREMENTS

Two approaches to the two-port PIM testing are employed in this study. They differ in both essential elements: the measurement instruments and the devices under test (DUT), which have dissimilar layouts of the printed lines. In Approach 1, the Summitek Instruments SI-900B PIM analyzer is used, whilst the test instrument in Approach 2 is assembled of the separate blocks, [9], including power sources, combiner, transmitter and receiver duplexers, filters, amplifiers, etc. Both instruments supply two continuous wave carriers of up to 2×44 dBm at frequencies f_1 and f_2, and record PIM level at the intermodulation frequency (3^{rd} order PIM signal P_{IM3} is monitored thereafter at frequency $f_{IM3}=2f_1-f_2$) at the reference planes 1 (reverse PIM - P_{IM3}^{rev}) and 2 (forward PIM - P_{IM3}^{fwd}) located at the connectors of the board launchers as shown in Fig. 1a. Both instruments have the certified receiver sensitivity better than -140 dBm.

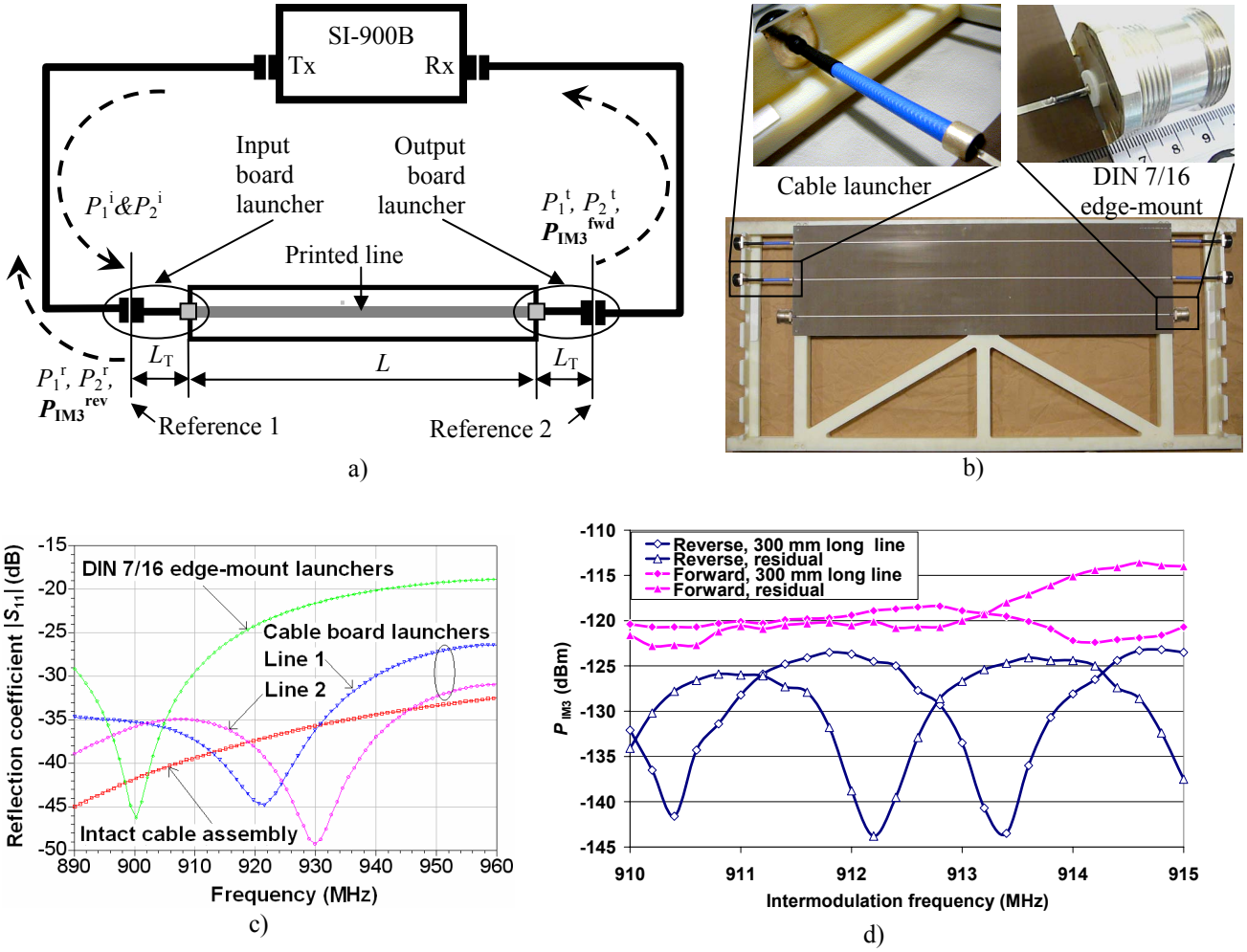

Fig. 1. a) Schematic of the two-port transmission/reflection intermodulation measurements; b) a view of the sample printed board on the test fixture and details of the board launchers: cable launcher (left insert) and DIN 7/16 edge-mount launcher (right insert); c) qualification of the board launchers on the reference microstrip lines (Board 1); and d) PIM characterisation of the cable launchers on the low PIM board (Board 2)

The test setups are usually calibrated by measuring the residual reverse PIM level when a low PIM load is connected to the instrument output port Tx. Alternatively, both reverse and forward residual PIM levels are measured when Tx and Rx ports are connected directly, see e.g. [3] and [10]. However to determine the actual residual PIM level of the whole setup, the contributions of the cables and connectors attached to DUT should be additionally taken into account. Therefore, the residual P_{IM3} levels have been determined here by replacing the DUT with a low PIM 7/16 THRU-standard. In the frequency band 910 to 914.8 MHz (GSM900 receiver band) at the input power 2×43 dBm, the residual P_{IM3} were measured below -130 dBm (reverse) and -125 dBm (forward). These data have enabled an estimation of the experimental uncertainty, which is obtained by the geometrical summation of the residual PIM signals of the instrument and DUT, cf. [11].

The DUTs tested with both approaches comprise the sections of 50 Ω printed lines. However, the types of launchers and the conductor layouts employed in these setups are fundamentally different, viz. soldered contacts are used in Approach 1, whilst contactless launchers are adopted in Approach 2 [9]. Most of the microstrip launchers require soldered joints to the signal and ground conductors, e.g. edge-mount DIN 7/16 launchers, [12], vertical cable launchers, [13], or horizontal cable launchers [14]. The first and last arrangements have been used in Approach 1, Fig. 1b. Each pair of the cable launchers in Fig. 1b was made by cutting in half a UT-250C-FORM semi-rigid coaxial cable assembly of length 25 cm and diameter 6.35 mm terminated into two DIN 7/16 flange mount connectors. The original assemblies have been PIM certified for reverse P_{IM3} level below -122 dBm at carriers' power 2×43 dBm in GSM900 band. After cutting the cable assembly and stripping its open ends, each half had 2.5 mm long central conductor protruding from the shield. Each stripped end was fitted with a transition unit, which was soldered to the ground conductor of the printed line, while the protruding central conductor was soldered to the signal strip. The transition units were lathed from bulk copper and plated by 5 μm immersion silver. These cable launchers are suitable for the use with both microstrip and coplanar waveguide lines. Also, Spinner DIN 7/16 edge-mount connectors shown in Fig. 1b have been used on the same

board for comparison. In this study, the connectors designed for 1.58 mm thick boards were used with the 0.76 mm thick boards.

The soldered microstrip launchers were tested in GSM900 band by measuring the reflection coefficient S_{11} on a triplet of 914 mm long straight uniform 50 Ω microstrip lines, Fig. 1b. The specimens were fabricated on a single board (Board 1) of Taconic RF-30 laminate of thickness 0.76 mm with low profile 35 µm thick copper cladding coated with 1 µm thick immersion tin. Two lines (Lines 1 and 2) were fitted with the cable launchers, while the third line (Line 3) had the edge-mount connectors. The measurement results in Fig. 1c show that the cable launchers exhibit better matching in the measurement band than the edge-mount connectors. The reverse and forward P_{IM3} measurements of a short 300 mm long straight uniform microstrip line (Line 4) fitted with two cable launchers were performed in the GSM900 band at carriers' power 2×43 dBm. The line was fabricated on the low PIM Taconic TLX-9 laminate of thickness 1.58 mm (Board 2) with the same conductor cladding as Board 1. Taking into account for ~5 dB drift of the measured P_{IM3} levels, results in Fig. 1d demonstrate negligible effect of the cable launchers on the PIM measurements.

The contactless microstrip launchers [9] in Approach 2 employ a broadside coupler shown in Fig. 2. This arrangement involves a special test fixture, as well as the coupler components printed on the board together with the test lines. The fixture consists of two parts made of bare aluminium: a solid milled frame and an upper bolted lid (not shown). Two 7/16 connectors provide external connection of the fixture, and two copper fins are used for coupling to the test board. The unique features of the fixture include vacuum clamping of the test board (through the holes in the bottom plate) and complete electromagnetic shielding when the upper lid is in place. The printed conductor layout comprises the elements of the broadside couplers, designed for -1 dB coupling, integrated with a section of the meandered uniform strip, (Fig. 2c). All conductors are printed on one side of the laminate, while the copper cladding is completely removed from the other side. Thus, the bottom plate of the test fixture acts as a ground conductor of the test board, and reliable tight contact between the test board and the fixture becomes critical for the PIM measurements in this test arrangement. The split tapered couplers in the printed layout were numerically optimized to provide return loss below -20 dB in the GSM900 band and satisfactory performance in portions of 1800-1900 MHz bands for the substrates with relative permittivity of 2.55.

The broadside couplers have been tested with the twin 50 Ω meandered microstrip lines (Lines 5 and 6) of length 1234 mm, fabricated on a single board (Board 3) of Taconic RF-30 laminate, Fig. 2c. The measured reflection coefficient in Fig. 2d demonstrates that matching in this case is worse than that on the lines 1-3, yet it is still reasonably good for the accurate P_{IM3} measurements. PIM characterisation of the couplers, performed with different laminate materials, has shown the lowest measured level of forward P_{IM3} to be about -120 dBm, which can be associated with the residual PIM level of the overall test setup including the instrument, feed cables and test fixture.

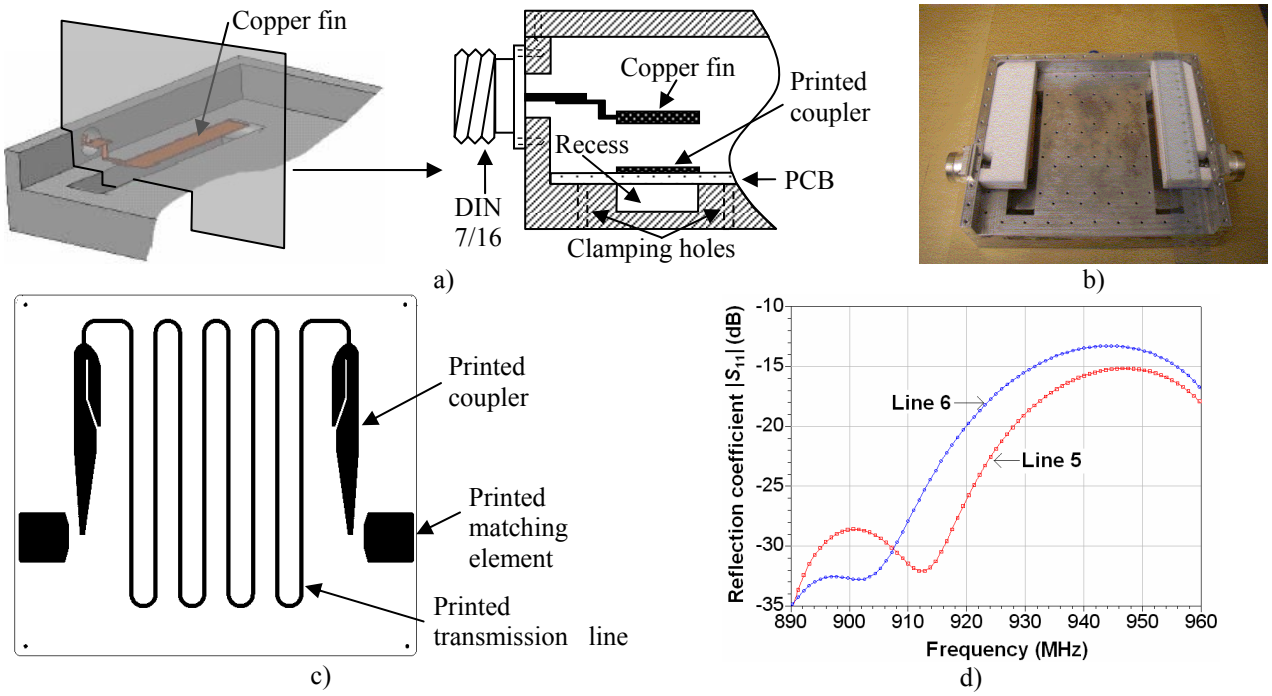

Fig. 2. Fixture for the contactless microstrip launchers in Approach 2. (a) elements of the broadside coupler in the test fixture; (b) fixture frame; (c) layout of the printed line specimen with integrated elements of the coupler; and (d) measured reflection coefficient.

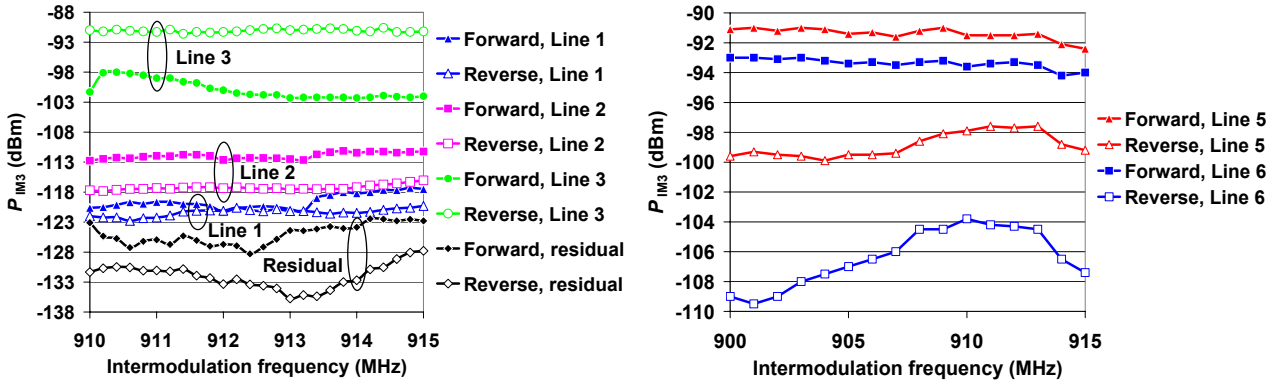

a) b)

Fig. 3. PIM products measured on Taconic RF-30 laminate using the Approaches 1 (a) and 2 (b).

The results of P_{IM3} measurements on the Taconic RF-30 laminate (Boards 1 and 3) obtained by using the Approaches 1 and 2 are presented in Fig. 3 for carriers' power 2×43 dBm and frequencies swept so that the 3rd order intermodulation frequency is in the GSM900 band. Cable loads have been used in the reverse PIM measurements. The following conclusions can be inferred from the measurement results:

- Both reverse and forward P_{IM3} levels on the line 3 with DIN 7/16 edge-mount connectors are considerably higher than those on the similar lines 1 and 2 with the cable launchers. Besides, in contrast to the lines 1 and 2, reverse P_{IM3} level on the line 3 is higher than forward P_{IM3} that suggests strong contribution of the edge-mount connectors to the measured PIM response, [15]. Therefore, matching of the test samples is a prerequisite for the adequate PIM characterisation, cf. [16]. Thus, the low reflection launchers should be used for PIM characterisation of PCB materials, and the scattering parameters of the test specimens should be monitored to assure high quality matching.
- PIM products measured on the two identical lines 1 and 2 with the cable launchers of same type differ for about 5 dB. The higher level of the PIM products on line 2 has been consistently observed for several different cable launchers. Such variations of P_{IM3} level occurred within the same test procedure (Approach 1) despite all care was taken to fabricate the identical specimens, which were concurrently manufactured on the same board and fitted with similar launchers. These results suggest that even minor dissimilarity of the printed traces arising in the course of the board fabrication and processing can considerably affect PIM performance of the printed circuits. To alleviate this problem and assess measurement uncertainty, a few replicas of the specimens should be tested in a series of reconnections.
- P_{IM3} levels on the lines 5 and 6 are higher than those on the lines 1 and 2. Whilst it still requires further investigation, such a discrepancy may result from the dissimilarity of the ground planes, different length of the strips and different printed layouts, as well as hail from the different production batches and time between fabrication and measurement of the lines used in Approach 1 (lines 1 and 2) and Approach 2 (lines 5 and 6).
- Discrepancy in P_{IM3} levels on lines 5 and 6 has been attributed to minor dissimilarities in the printed lines and the broadside directional couplers. Besides, significant dependence of the discrepancy with time after etching (ageing) and on storage conditions has been observed.

Comparison of the measurement results obtained for the same laminates by the independent Approaches 1 and 2 has demonstrated that PIM characterisation of PCB is highly sensitive to matching of the test specimens and the type of launchers used. Therefore, for consistent evaluation of PIM performance of PCB materials it is advisable to make comparative measurements within a single technique. It is also noteworthy that the possibility of swift DUT replacement in Approach 2 offers apparent advantages for the comparative production testing of the materials. Despite all the constraints and shortcomings, the two-port reflection/transmission PIM measurements still remains the only technique which provides sufficient sensitivity for evaluation of low PIM laminates. Alternatively, near-field mapping of PIM product distributions on printed lines can be used to gain insight into the mechanisms of PIM generation as described in the next section.

2. NEAR-FIELD MAPPING OF INTERMODULATION PRODUCTS

The schematic of the near-field probing setup based on the SI-900B PIM analyzer is shown in Fig. 4a. In contrast to the two-port measurements, the DUT output is now terminated in the low PIM matched load, while the input of the PIM analyzer is connected to the *E*-field probe. A 112 m long SUCOFORM-141-CU-FEP cable load provides residual reverse P_{IM3} level below -130 dBm at carriers' power 2×43 dBm in the GSM900 band. The capacitive *E*-field probe is shown in Fig. 4b. It is made of 6.35 mm diameter semi-rigid coaxial cable with the tip formed by the inner conductor

protruding from the shield for 6 mm. The probe is oriented normally to the surface and picks up predominantly vertical component of the electric field E_z. To ensure the constant spacing of 0.7 mm between the probe tip and the board surface the probe tip is encapsulated into a polyethylene sleeve of length 6.7 mm cut from the insulating spacer of coaxial cable RG58/U. Length of the probe tip and spacing has been chosen, by cut and try method, to provide sufficient sensitivity at minimum perturbation to the measured field.

The probe, pressed against the board surface, may alter the actual PIM product distribution by causing:

- a localised discontinuity, which may affect the field pattern on the test line - this effect is essentially linear and therefore can be characterised by the linear scattering parameters, cf. [17];
- a localised PIM source, because the probe is exposed to the high-power carriers.

These effects have been assessed through the near-field probing of the 915 mm long straight uniform 50 Ω microstrip line, Line 7, fabricated on the Taconic TLG-30 substrate of thickness 0.76 mm, with copper cladding and finished with 1 μm thick immersion tin (similar to RF-30 laminate above). The cable launchers have been employed to feed the printed line. The probe was first characterised in the linear regime by *S*-parameters measured versus the probe position along the reference line (the VNA is used in place of the PIM analyser in the test setup shown in Fig. 4a).

The probe coupling to line specimens have been evaluated in the following three arrangements:

i. Vertical *E*-probe 1 with 6 mm tip covered by 6.7 mm long sleeve made of the cable insulating spacer (wall thickness 1.2 mm) as described above. This probe is used further in section 3.
ii. Vertical *E*-probe 2 with 6 mm tip covered by 6.7 mm long tubular pen refill (wall thickness 0.6 mm).
iii. Horizontal *E*-probe without cover; the tip is elevated for 2.5 mm above the substrate surface.

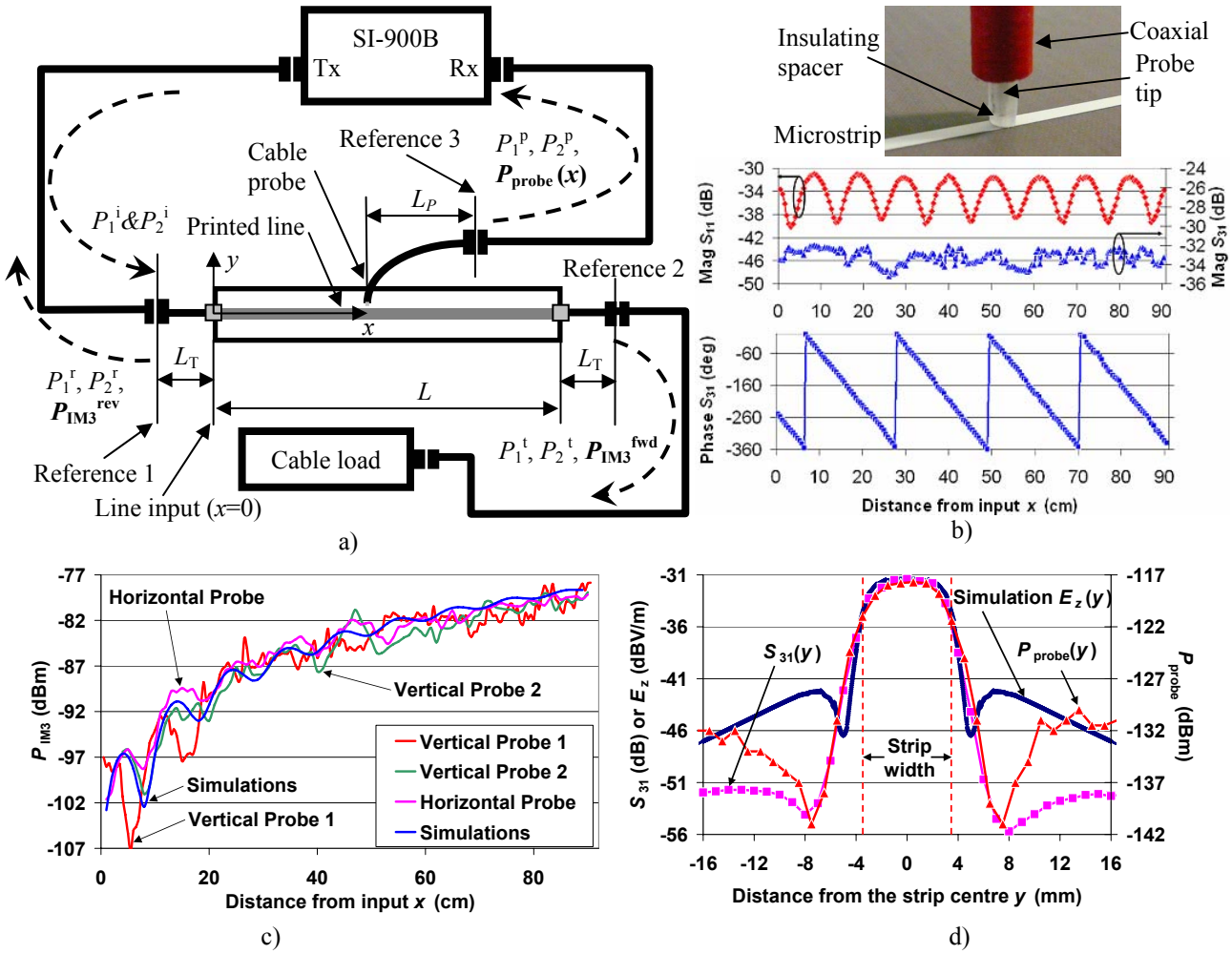

Fig. 4. (a) Schematic of the PIM near-field probing setup; (b) characterisation of the vertical *E*-probe 1 in the linear regime at the 3rd order PIM frequency of 910 MHz; (c) near-field mappings of PIM product distributions along the microstrip line of width 1.9 mm obtained with the three different probe arrangements; d) measured cross-sectional distributions of PIM level P_{probe}, linear probe coupling S_{31} and simulated vertical electric field E_z at height 0.7 mm above the strip on the microstrip line of width 7.44 mm.

To avoid ambiguity in the probe positioning, the vertical probes were positioned along the strip centre line, while tip of the horizontal probe was placed across the strip. Since the probe coupling varied from one arrangement to another, it was characterised for each probe configuration by the linear transmission magnitude S_{31}. Measurement results for the vertical probe 1 located at the centre of the printed trace shown in Fig. 4b demonstrate low return loss (S_{11}<-30 dB), nearly constant weak coupling (S_{31}<-32 dB) and linear phase variation (Phase S_{31}) along the line. Small deviations of S_{31}, less than ±1.5 dB, from the mean value as the probe moves along the trace are attributed mainly to uncertainty of the probe positioning and small mismatch of the line terminals. Therefore, the mean value of S_{31} measured along the centre of microstrip trace has been adopted as a representative quantity of the probe coupling to microstrip line, viz. $P_{cpl}=<S_{31}>$. These results also suggest that the probe inflicts only minor perturbation of the near-field distribution of the carriers guided by the printed microstrip line.

In the nonlinear regime, impact of the probe has been assessed by comparison of the PIM distributions along the reference line. For the three probe arrangements (i)-(iii) above, P_{cpl} measured at frequency of 910 MHz are -33.2 dB, -33.1 dB and -39.6 dB, respectively. Then the actual level of $P_{IM3}(x)$ at point x referenced to the line input, Fig. 4a, can be de-embedded from the near-field probing as follows: $P_{IM3}(x)=P_{probe}(x)-P_{cpl}$, where $P_{probe}(x)$ is the probe reading at distance x from the line input. The PIM distributions along the microstrip Line 7 acquired with the three probe arrangements (i)-(iii) are shown in Fig. 4c. All the plots exhibit good agreement of the mapped P_{IM3} distributions, albeit a minor offset can be observed between the results for the vertical probes 1 and 2. This offset is associated with different interconnecting cables used in these two measurements and thus provided slightly dissimilar matching conditions at the reference planes 1 and 2. Nevertheless, such a good correlation of the P_{IM3} distributions testifies weak effect of the probe on the measured field and provides the evidence of the linear probe response. Negligible contribution of the probe itself to the measured PIM products becomes even more apparent from the comparison of the P_{IM3}^{fwd}=-80.1 dBm measured in the two-port transmission test with the results of the near-field probing at the strip end $P_{IM3}(x=L)$=-78.9 dBm. A small discrepancy between the values of P_{IM3}^{fwd} and $P_{IM3}(x=L)$ is attributed to the fact that the respective readings are taken at different reference planes.

To assess resolution and sensitivity of the near-field probing setup, PIM product distributions have been mapped across a microstrip line of width 7.44 mm fabricated on the Taconic TLG-30 laminate of thickness 0.76 mm (the collar-shaped strip of width 7.44 mm and length 515 mm was matched to 50 Ω feeder microstrip lines of width 1.9 mm using tapered transformers). The results of the near-filed mapping of the 3rd order intermodulation products at frequency 910 MHz and carriers' power 2×44 dBm are shown Fig. 4d in comparison with the linear near-filed mapping of the transmission magnitude S_{31} at 910 MHz and simulated pattern of the vertical component of electric field at the height of the probe tip. All distributions have the similar bell shape with maximum at the strip centre but the dips of the mapped distributions are slightly offset from the theoretical ones. The latter discrepancy can be attributed to the contribution of horizontal components of electric field and the effect of the tip length and diameter, [18]. Nevertheless, these observations demonstrate that the chosen probe geometry provides good spatial resolution suitable for mapping PIM product distributions in complex layouts of printed circuits.

It is necessary to note that while the near-field probing allows direct observation of PIM products, its applicability is restricted by sensitivity of the PIM analyser. The requirement of the weakly coupled probe effectively raises the limits of the P_{IM3} measurements by nearly 30 dB, as compared to the two-port measurements using the same instruments.

3. CORRELATION BETWEEN TWO-PORT AND NEAR-FIELD CHARACTERISATION TECHNIQUES

PIM products are generated at each point of the printed line and are guided in both forward and reverse directions. On the matched lines, the quantities P_{IM3}^{fwd} and P_{IM3}^{rev} represent magnitudes of the forward and reverse travelling PIM signals, which are measured separately at the DUT terminals when using the two-port setup (Approaches 1 and 2). In contrast, $P_{probe}(x)$ obtained by the near-field probing represents the magnitude of the total field at point x which is a superposition of the PIM products travelling in opposite directions.

In order to illustrate the features of these characteristics, the results of the two-port measurements (Approach 1) of P_{IM3}^{fwd} on microstrip lines of the length varied from 10 to 195.5 cm and near-field mapping on the 195.5 cm long line are superimposed in Fig. 5. The samples of the uniform 50 Ω microstrip lines were fabricated on the Taconic TLG-30 laminate, and the tests were performed at carriers' power 2×44 dBm and intermodulation frequency f_{IM3}=910 MHz (f_1=935 MHz and f_2=960 MHz). Results of the two-port measurement in dBm have been averaged over a series of 3 reconnections of each microstrip line.

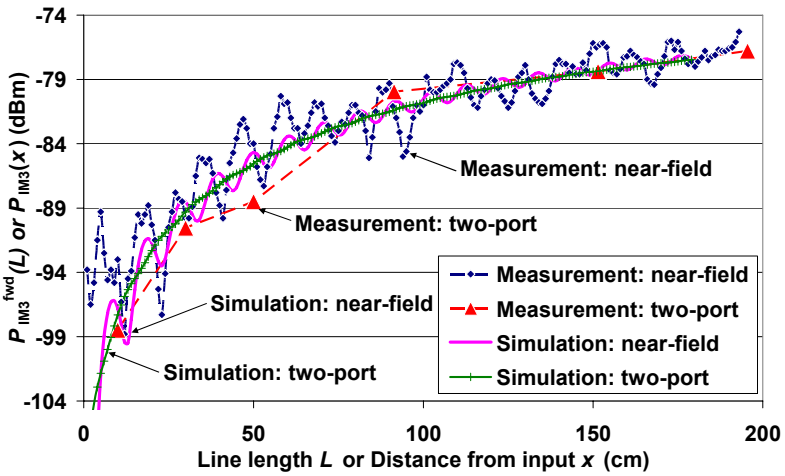

Fig. 5. Comparison of P_{IM3}^{fwd} level on the microstrip lines of several lengths measured with the aid of Approach 1 against $P_{IM3}(x)$ distribution along the line mapped with the near-field probing.

It is important to note that the level of P_{IM3}^{fwd} on the 195.5 cm long line is close to the corresponding normalised reading of the probe, where a small discrepancy is associated with the offset of the reference planes. The near-field distribution of PIM products shows noticeable regular ripples, while the results of the two-port measurements exhibit monotonic growth of P_{IM3}^{fwd} level with the line length. These observations are in good agreement with the simulations based on the nonlinear transmission line model of distributed nonlinearity in printed lines, [7]. The phenomenological parameters of the model, such as the nonlinear resistance per unit length and port reflection coefficient, have been fitted to the experimental data of Fig. 4c. The rationale behind the use of the phenomenological parameters fitted to the results in Fig. 4c for the simulations in Fig. 5 is to verify the model and prove that the extracted parameters are representative of a given laminate and are applicable to simulation of the intermodulation response of different planar structures manufactured of this specific material. It needs to mention here that the port reflections intensify and displace the ripples on the near-field distributions, [19], and also distort the cumulative curve of the output forward PIM products. Fig. 5 provides conclusive evidence of the distributed nature of the nonlinearity of the measured printed line samples, as the cumulative intensification is inherent to the travelling wave harmonic generation in a nonlinear medium [7], [20].

4. CONCLUSION

Two-port reflection/transmission measurements and near-field mapping of PIM products in printed transmission lines have been applied to characterisation of PIM performance of PCB laminates. The two-port measurement setups based upon two different test fixtures with contactless and soldered cable launchers have exhibited noticeably different absolute level of PIM products in the same laminate material. Nonetheless the measurement results remain consistent within each setup, and the same qualitative behaviour of PIM products is observed in both setups. Therefore, for reliable characterisation of PIM performance of PCB materials, it is necessary to carry out comparative measurements of the printed lines using the same test setup. It was observed in the two-port measurements that even minor dissimilarity of the printed line specimens can cause significant variations of the PIM level and thus affect measurement uncertainty. This suggests that the statistical approach should be used to determine representative PIM characteristics of each laminate material with reference to the specific layout of printed conductors. In this respect the contactless launching has proved to be more advantageous technique for the production testing of PCB materials.

Near-field probing of PIM product distributions on printed lines has been used to gain insight into the mechanisms of PIM generation in printed lines. The presented mappings of PIM products are consistent with the two-port measurements and clearly show the cumulative growth of PIM level with the line length. The results of near-field probing have explicitly demonstrated that mismatch of the printed lines inflicts variations in the PIM level along the microstrip lines (ripples on plots in Fig. 5).

ACKNOWLEDGEMENTS

This work is supported by the UK Engineering and Physical Science Research Council under the grant EP/C00065X/1. Authors are grateful to Taconic Advanced Dielectric Division Ltd, Trackwise Designs Ltd, PCTEL Inc, and Castle Microwave Ltd for their help in sample manufacturing and providing test facilities. Special thanks go to Mr J. Francey for his continuous support and to Mr N. Carroll for his help with the measurements. Authors also wish to acknowledge the advice provided by Dr D. Linton and Dr O. Malyuskin of Queen's University of Belfast over the period of the work.

REFERENCES

[1] B. Deats and R. Hartman, “Measuring the passive intermodulation performance of RF cable assemblies,” *Microwaves & RF*, pp. 108-117, March 1997.

[2] J. Verspecht and P. Van Esch, “Accurately characterizing hard nonlinear behavior of microwave components with the nonlinear network measurement system: Introducing ‘nonlinear scattering functions,” in *Proc. 5th Int. Workshop Integrated Nonlinear Microwave Millimeterwave Circuits*, Germany, October 1998, pp. 17–26.

[3] Passive intermodulation measurement techniques, Application Notes, Summitek Instruments, Inc., May 1999. [Online]. Available: www.summitekinstruments.com.

[4] M. Bayrak and F. A. Benson, "Intermodulation products from nonlinearities in transmission lines and connectors at microwave frequencies," *Proc. IEE*, vol. 122, no. 4, pp. 361-367, April 1975.

[5] C. Vicente and H. L. Hartnagel, "Passive-intermodulation analysis between rough rectangular waveguide flanges," *IEEE Trans. MTT*, vol. 53, no. 8, pp. 2515-2525, August 2005.

[6] J. A. Jargon, D. C. DeGroot, and K. L. Reed, “NIST passive intermodulation measurement comparison for wireless base station equipment,” *52nd ARFTG Conference Digest*, vol. 34, pp. 128-139, December 1998.

[7] D. E. Zelenchuk, A. P. Shitvov, A. G. Schuchinsky and T. Olsson, “Passive Intermodulation on Microstrip Lines,” in *Proc. of the 37th European Microwave Conference*, Munich, Germany, October 2007, pp. 396-399.

[8] A. P. Shitvov, D. E. Zelenchuk, A. G. Schuchinsky, V. F. Fusco and N. Buchanan, “Mapping of passive intermodulation products on microstrip lines,” in *Proc. of IEEE MTT-S IMS’08*, Atlanta, Georgia, June 2008.

[9] J. V. S. Perez, F. G. Romero, D. Rönnow, A. Söderbärg, T. Olsson, “A microstrip passive intermodulation test set-up; comparison of leaded and lead-free solders and conductor finishing,” in *Proc. MULCOPIM 2005*, Noordwijk, The Netherlands, September 2005, pp. 215-222.

[10] Z. Zhiqiang, L. Fumin, S. Wen, “Exploration for the calibration of passive intermodulation analyzer,” in *Proc. ICEMI’2007*, Xi’an, China, August 2007, vol. 1, pp. 46-49.

[11] Passive Intermodulation Distortion Analyzer: Operating and Maintenance Manual, Summitek Instruments, 2004.

[12] A. G. Schuchinsky, J. Francey and V. F. Fusco, “Distributed sources of passive intermodulation on printed lines,” in *Proc. 2005 IEEE Ant. and Prop. Soc. Int. Symp*., Washington DC, USA, July 2005, vol. 4B, pp. 447-450.

[13] N. Kuga and T. Takao, “Passive intermodulation evaluation of printed circuit board by using 50Ω microstrip line,” in *Proc. APMC 2004*, New Delhi, India, December 2004.

[14] A. P. Shitvov, D. E. Zelenchuk, A. G. Schuchinsky and V. Fusco, “Passive intermodulation in printed lines: effects of trace dimensions and substrate,” *Trans. IET MAP* [in press].

[15] A. P. Shitvov, D. E. Zelenchuk, A. G. Schuchinsky and V. Fusco, “Passive intermodulation generation on printed lines: near-field probing and observations,” *IEEE Trans. MTT Special Issue on the 2008 International Microwave Symposium* [unpublished].

[16] D. E. Zelenchuk, A. P. Shitvov and A. G. Schuchinsky, “Effect of matching on passive intermodulation in transmission lines with distributed nonlinear resistance,” in *Proc. EMTS 2007*, Ottawa, Canada, July 2007

[17] P. Kabos, H. C. Reader, U. Arz, and D. F. Williams, "Calibrated waveform measurement with high-impedance probes," *IEEE Trans. MTT*, vol. 51, no. 2, pp. 530-535, February 2003.

[18] D. Baudry, A. Louis, and B. Mazari, “Characterization of the open-ended coaxial probe used for near-field measurements in EMC applications,” *Progress In Electromagnetics Research,* PIER 60, 311–333, 2006.

[19] D. E. Zelenchuk, A. P. Shitvov, A. G. Schuchinsky and V. Fusco, “Passive intermodulation in finite lengths of printed microstrip lines,” *IEEE Trans. MTT Special Issue on the 2007 European Microwave Conference* [unpublished].

[20] N. Bloembergen, *Nonlinear Optics*, New York – Amsterdam, W. A. Benjamin, Inc., 1965.